Proceedings of the ASME Turbo Expo 2020
GT2020
June 22-26, 2020, London, England

GT2020-14714

ICE CRYSTAL ICING INVESTIGATION ON A HONEYWELL UNCERTIFIED RESEARCH ENGINE IN AN ALTITIUDE SIMUATION ICING FACILITY

Ashlie B. Flegel
NASA Glenn Research Center
Cleveland, Ohio, USA

ABSTRACT

A Honeywell Uncertified Research Engine was exposed to various ice crystal conditions in the NASA Glenn Propulsion Systems Laboratory. Simulations using NASA's 1D Icing Risk Analysis tool were used to determine potential inlet conditions that could lead to ice crystal accretion along the inlet of the core flowpath and into the high pressure compressor. These conditions were simulated in the facility to develop baseline conditions. Parameters were then varied to move or change accretion characteristics. Data were acquired at altitudes varying from 5 kft to 45 kft, at nominal ice particle Median Volumetric Diameters from 20 μm to 100 μm, and total water contents of 1 g/m^3 to 12 g/m^3. Engine and flight parameters such as fan speed, Mach number, and inlet temperature were also varied. The engine was instrumented with total temperature and pressure probes. Static pressure taps were installed at the leading edge of the fan stator, front frame hub, the shroud of the inlet guide vane, and first two rotors. Metal temperatures were acquired for the inlet guide vane and vane stators 1-2. In-situ measurements of the particle size distribution were acquired three meters upstream of the engine forward fan flange and one meter downstream of the fan in the bypass in order to study particle break-up behavior. Cameras were installed in the engine to capture ice accretions at the leading edge of the fan stator, splitter lip, and inlet guide vane. Additional measurements acquired but not discussed in this paper include: high speed pressure transducers installed at the trailing edge of the first stage rotor and light extinction probes used to acquire particle concentrations at the fan exit stator plane and at the inlet to the core and bypass. The goal of this study was to understand the key parameters of accretion, acquire particle break-up data aft of the fan, and generate a unique icing dataset for model and tool development. The work described in this paper focuses on the effect of particle break-up. It was found that there was significant particle break-up downstream of the fan in the bypass, especially with larger initial particle sizes. The metal temperatures on the inlet guide vanes and stators show a temperature increase with increasing particle size. Accretion behavior observed was very similar at the fan stator and splitter lip across all test cases. However at the inlet guide vanes, the accretion decreased with increasing particle size.

INTRODUCTION

A key goal of NASA's engine icing research is to understand the physics of the ice-crystal icing phenomenon in order to develop models that can predict ice accretion and inform current and future propulsion designs of potential icing or certification challenges. NASA Glenn has been building an understanding of the fundamental ice-crystal icing physics through a series of tests conducted on a NACA0012 airfoil in two altitude icing facilities [1-6]. This work formed the basis of the icing risk criteria used in the development of the NASA in-house 1D Icing Risk Analysis tool, COMDES-MELT [7-11].

Research continues, among the icing community, to understand the ice crystal particle behavior in an engine for the development of particle break-up and trajectory models [12-16]. Most tests have been carried out using static test articles. Knezevici et al. [12] conducted an ice accretion test on an inter-compressor duct bleed slot and observed the role of ice particle size. The authors noted by decoupling the role of particle melt, the larger end of the particle size distribution plays a more significant role in the magnitude of the ice accretion for wet bulb temperatures above and below freezing. Additionally, the authors suggested that ice erosion increased with particle size.

The break-up phenomena in an engine environment is quite complex and the environment varies as the particle is ingested into the engine. Several investigations on the microscale level have tried to look at these break-up characteristics. Representative of a particle impacting the fan or initial stages of an engine (i.e dry, cold surface), Hauk [13,14] examined the break-up characteristics of spherical and non-spherical ice particles ranging from 0.03mm to 3.5mm impacting on a flat plate. The ambient temperature and surface temperature ranged from −10º to −20º C. The study also investigated velocity and impact angles. Four different fragmentation characteristics were

observed and this led to a particle collision and fragmentation model. This work lead to an understanding that most collisions with rotating turbo machinery is likely to produce "catastrophic" breakup leading to very small particles being ingested into the engine.

Representative of a particle impacting further downstream in an engine (i.e. dry, warm surface), Vargas et al. [15] conducted a parametric study of the fragmentation behavior of particles ranging from 2 mm to 3 mm impacting a warm flat plate. The flat plate temperature was at 22.4°C and the particle temperatures ranged from −6°C to −16°C. Additional parameters studies included varying velocities from 40 to 80 m/s and target angles from 5 to 90 degrees.

As a particle enters the engine and melt begins to occur, a water film or runback water begins to form on the stationary surfaces. Hauk [16] performed initial studies on particle impacts on a thin water film. This study observed the break-up characteristics over a range of particle sizes (1.18 mm to 3.52 mm), impact velocities (1.2 to 5.8 m/s), and water film thickness (130 to 600 μm). The authors found that cases with no fragmentation had a velocity that was two times higher compared to dry target cases from [13,14].

Particle break-up has also been observed on a rotating target. Vargas et al. [17] studied spherical particle break-up (1.5mm to 3mm) on a wedge attached to a rotor. The wedge angles were varied between 0º to 60°. The data show that the fragmented particle velocities are higher at the edge of the impact cloud. At these higher velocities, the impact had a lower bounce normal to the wedge compared to the motion of the fragments along the surface. The authors found that these findings compared very well to the literature on hailstone impacts.

Limited data exists on a full scale engine due to the complexity of the tests and lack of facilities with altitude ice-crystal capability. NASA Glenn, in collaboration with Honeywell and participation from the Ice Crystal Consortium, previously conducted two test campaigns on an unmodified ALF502R-5 engine configuration [18-21]. Those studies gave an initial understanding of ice-crystal accretions in a relevant environment. However this engine was an older design and featured a heated spinner which provided an additional source of liquid due to melting of impacting ice crystals. Note that the presence of liquid water is believed to be a prerequisite for the formation of icing within the compressor during ice crystal icing. The data from these tests led to the development of an icing risk criteria that the 1D Icing Risk Analysis tool (COMDES-MELT) uses to determine if a simulated condition has a potential risk of icing in an engine core flowpath [10]. Initial 3D simulations using LEWICE3D were also conducted to evaluate the tool's ability to simulate the break-up and heat transfer effects inside the engine [22-24].

This present study looks at a different engine geometry with a hidden core design. The research engine was never in production so there are not any known ice-crystal icing issues. Therefore it provided an ideal testbed for the 1D Icing Risk Analysis tool to perform an assessment to determine any potential icing risk [25]. Additionally, new icing measurement techniques were assessed to provide insight on the ice cloud state in the engine.

The objective of this present study focused on developing an understanding of particle behavior through an engine, evaluate the effectiveness of using a 1D Icing Risk Analysis tool to predict ice accretion, and develop a dataset for model and tool development. One particular dataset of interest, and is described in this paper, looks at the engine and cloud effects for three different MVD (particle size) sweeps. Particle distributions from the High Speed Imaging instrument, video images, and engine temperature trends are presented in the results.

Typically in the natural environment, ice crystal particle sizes are on the order of $d_{v,0.50}$ = 250μm-1000μm [26]. The PSL facility is limited to smaller particle size, however break-up effects from impacts with the fan and engine components likely result in smaller particle sizes within the engine core. In addition to acquiring data on particle break-up for model development, there is this added interest to understand the particles break-up from the fan and how much the initial cloud distribution at the inlet effects the downstream distribution.

NOMENCLATURE

Alt	altitude [kft]
BCPD	back-scatter cloud polarization detection
$d_{v,\,0.XX}$	percentile cumulative volume diameter
EGV	exit guide vane
HPC	high pressure compressor
HSI	high speed imaging instrument (Artium)
IGV	inlet guide vane
MFLT	flight Mach number
MVD	median volumetric diameter [μm]
N1	fan speed [rpm]
N2	core speed [rpm]
PSL	propulsion systems laboratory
Rdg	test point number
T_{amb}	ambient temperature, static [°C, °F]
T_{wb}	static wet bulb temperature [°F]
TWC	total water content [g/m^3]

DESCRIPTION OF EXPERIMENT

Facility Description

The Honeywell Uncertified Research Engine ice-crystal icing test was conducted in the NASA Glenn Research Center Propulsion Systems Laboratory Cell 3 (PSL-3). This facility has been used to conduct a wide variety of tests on turbofan, turboshaft, turbine-based combine cycle, and unmanned aerial vehicle engines for both commercial and military application since the early 1970s. PSL-3 is a direct-connect altitude test chamber that was modified with an icing system in 2010 [27]. A notional facility configuration with an engine installed is shown

in Figure 1. Details on the facility capabilities can be found in the PSL Customer Guide [28] and in Table 1.

PSL-3 can generate ice-crystals conditions through a freeze out method. This method produces a spherical ice crystal particle. The plenum chamber contains a spray bar system that has 222 independently controlled nozzles. Two types of nozzles are featured on this system, Standard nozzles used for higher water content conditions and Modified 1 nozzles, which have a smaller water tube diameter and are typically used for lower water content sprays. These nozzles are in a fixed, alternating pattern across each spray bar. The facility icing operation envelope is illustrated in Figure 2 overlaid on the FAA 14 CFR Parts 25 and 33 Appendix D envelope [29]. This study contained ice-crystal conditions that spanned across and outside the typical Appendix D icing envelope, shown in Figure 2a. Prior to the engine test, a series of tests were conducted to characterize the cloud for the requested icing conditions and gain further facility experience by exploring the PSL parameter space. Details of this characterization can be found in [30].

The TWC values described in this paper are based on center-line measurements of an Iso-Kinetic probe (IKP-2) at the exit of the calibration duct. The IKP-2 measurements were combined with the concentration factor from the inlet tomography to obtain a bulk TWC [30]. The TWC values for this test can be seen in Fig. 2b as the purple triangles.

During the test, the controlled facility parameters were held to the following tolerances:

Flight Mach number:	+/- 0.02
Temperatures:	+/- 1º F
Pressures:	+/- 0.05 psia
TWC:	+/- 1 g/m3

The total water content tolerance increased for altitudes below 30kft. Details on the Propulsions Systems Laboratory facility measurement uncertainty can be found in the following report [31].

For this test, the cloud nozzle pattern spanned across the entire PSL duct. Periodically during each run, the cloud uniformity would be observed and documented by the laser extinction tomography system [32].

Test Article Description

The Honeywell Uncertified Research Engine is a turbofan engine that features a hidden core design. This design with an inlet gooseneck feature helps keep the core less exposed, see Figure 3. The engine geometry featured a large front frame strut and the gooseneck led to a four stage high pressure compressor (HPC), so no booster or low pressure compressor was used in this configuration. Additional engine details can be found on Table 2.

The research engine had never been previously run under icing conditions so there was no background information how the engine would behave in ice crystal icing. Therefore, caution had to be taken to ensure the safety of the engine. Additionally the internal cameras and other instrumentation had limited life, therefore the researchers had to optimize the time the engine ran with the icing cloud on. To find icing points of interest, the facility was configured to run an icing condition predicted by the 1D Icing Risk Analysis tool. The ice cloud would be turned on and the researchers would observe the cameras for accretion and the engine metal temperatures. Once the metal temperatures reached a steady state and no further ice accretion was observed, the cloud was turned off. Spray times ranges from 60 seconds to 5 minutes. It was found during the test that none of the ice crystal conditions resulted in enough accretion to cause concern to the engine.

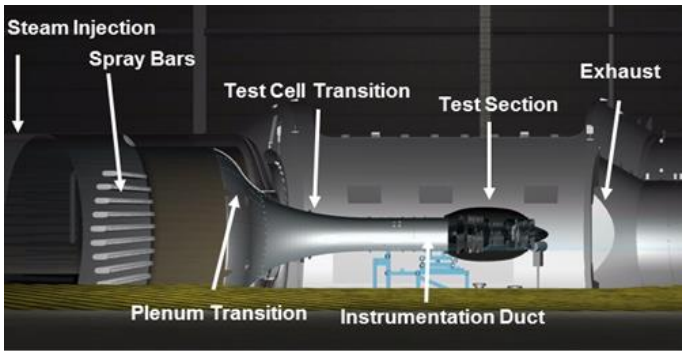

Figure 1. PSL-3 Facility Layout with Notional Engine Installation

Table 1. PSL-3 Capability

Specification	Min	Max
Engine / Rig Dia. (in | cm)	24 | 60	84 | 215
Air Flow Rate (lbm/s | kg/s)	10 | 5	330 | 150
Altitude, pressure (kft | km)	5 | 1.2	50 | 15
Total Temp (°F | °C)	-60 | -50	50 | 10
Mach Number	0.15	0.80
TWC (g/m^3)	0.3	~12.0
MVD (um)	15	>100 #

Maximum particle size is dependent on specific test point and facility conditions.

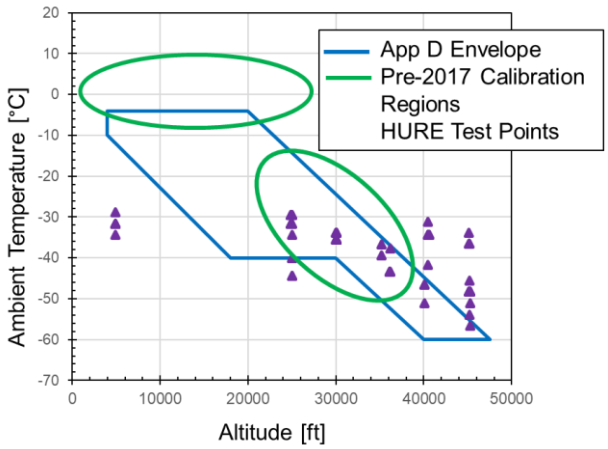

a.) PSL Envelope: Ambient Temperature vs. Altitude

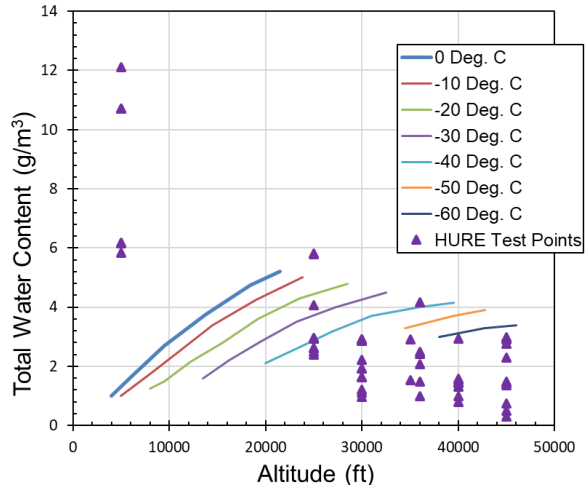

b.) PSL Envelope: Total Water Content vs. Altitude for Ambient Temperature Conditions. ***(TWC curves based on Appendix D Envelope, [29])***

Figure 2. PSL-3 Icing Envelope with Icing Conditions Tested.

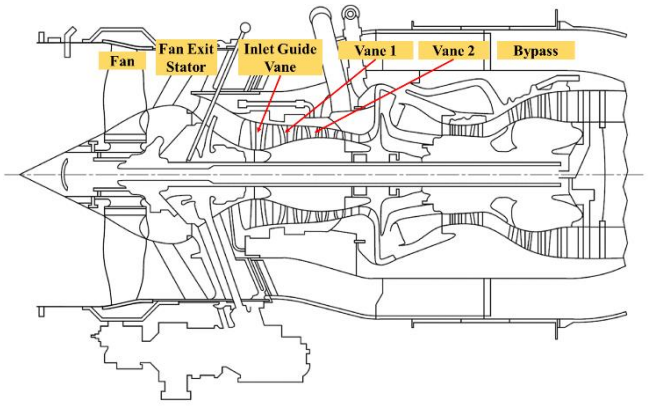

Figure 3. Honeywell Uncertified Research Engine cross-section.

Table 2. Engine Details

Parameter	Value
Bypass Ratio	4.2:1
Fan Diameter	34.2 in (0.87 m)
Engine Length	61.7 in (1.57 m)
Maximum T/O Thrust	8025 lb (3640 kg)
Fan Type	Direct Drive
Axial Compressor (# of stages)	4
Centrifugal HPC (# of stages)	1
High Pressure Turbine (# of stages)	2
Low Pressure Turbine (# of stages)	3

Measurement Description

The engine was fully instrumented with typical aero-research instrumentation. This paper will only describe the instrumentation critical to the ice-crystal assessment. Static pressure data were obtained on the front frame hub leading and trailing edge and along the outer shroud at Rotors 2 and 3. See Figure 4. At each axial location there were four static taps spaced evenly apart. Metal temperature data were acquired at four circumferential locations (labeled as A,G,N,U) at the inlet guide vane (IGV), and vanes 1 and 2. The thermocouples were located on the mid-span of the vane near the outer shroud.

Icing research instrumentation is shown in Figure 5. Humidity measurements were obtained at the core inlet and in the HPC exit.

Five high-speed pressure transducers, Kulites, were installed at the trailing edge of Rotor 1. The Kulites were in the same axial plane, spaced evenly apart in a 90° arc.

Light extinction tomography was used to non-intrusively monitor cloud uniformity at the engine fan face [30]. The tomography plane is located 1.5 meters in front of the engine. Light Extinction Probes (LEP) were used to understand particles aft of the fan. The LEP is a non-intrusive system that measures

line attenuation of light between the transmitter and receiver. The goal of these probes is to observe particle, shed ice, liquid, and/or liquid/ice slush runback transits, and determine TWC while the cloud is on. Analysis and development of this measurement is still underway. As shown in Fig. 5, the LEPs were located in a plane just aft of the fan and at the inlet of the core and bypass. During this study, there were issues with core inlet LEP. Only data from the fan exit and bypass inlet planes were available.

A key measurement for this study was to understand spherical particle break-up through an engine. Artium Technologies, Inc. High Speed Imaging (HSI) instruments and Droplet Measurement Technologies, Inc. (DMT) Back-scatter Cloud Probes with Polarization Detection (BCPD), were placed at the engine inlet and aft of the fan in the bypass flow to measure particle size (Fig. 5). This is a new approach for such instrumentation. Typically these types of instrumentation are used in external flow configurations, such as on the wing of a plane or in an open wind tunnel. The BCPD data were not available at the time of publication, so this paper focuses on the HSI measurements only. The HSI instruments were located three meters upstream of the fan face and one meter downstream of the fan face in the bypass flow. The particle size distributions acquired in a sampling volume at the centerline of the measurement plane. More specific details on the HSI measurements during this test and limitations can be found in King et al. [33]. It should be noted, the lower measurement limit of the HSI instrument used is 15µm. This leads to a bias and truncation in the data when the particle size distribution approaches this lower limit.

To observe ice accretions, there were four circumferentially spaced video cameras looking from the casing towards the hub of the fan exit stators. There was also one camera looking at the splitter lip and one camera downstream at the IGV. These three camera locations are shown in Figure 5. In addition, there were also cameras for general observation looking at the spray bars, fan spinner, fan blades, and at the inlet temperature sensors.

Test Conditions

The goal of this study was to generate an ice crystal icing dataset on a hidden core engine geometry. This test had a particular focus on understanding the particle break-up behavior aft of the fan and evaluating the effectiveness of using a 1D Icing Risk Analysis tool, COMDES-MELT. Additionally, this study looked at the accretion behavior in the engine over a range of flight and engine parameters (Fig. 2).

For these tests, a fully glaciated ice crystal cloud was generated through freezing out of the liquid water droplets from the spray bars. This results in spherical glaciated ice particles. Untreated city water was used during the test to promote nucleation and a constant plenum relative humidity of 45% was used throughout the test. The cloud diameter was such to cover across the entire span of the duct.

The conditions covered in this test can be found documented as a function of ambient temperature (Fig 2a) and total water content (Fig 2b) versus altitude in Figure 2. This paper will focus on three particle size sweeps which are described in Table 3 and Table 4.

Three MVD sweeps were performed for three engine conditions based on predictions from the 1D Icing Risk Analysis and showed ice accretion during initial cloud sprays at the beginning of testing. For each sweep, the engine, flight, and cloud conditions including TWC were held constant.

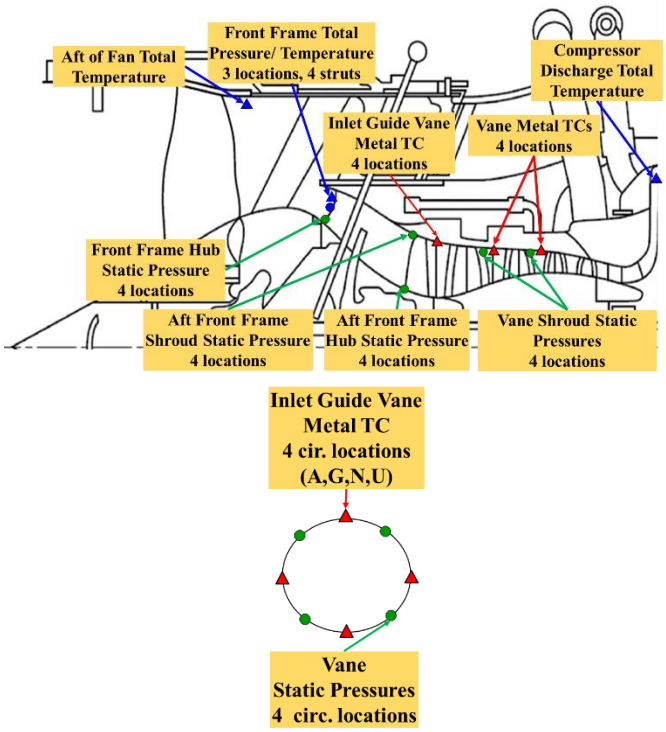

Figure 4. Engine Instrumentation Schematic.

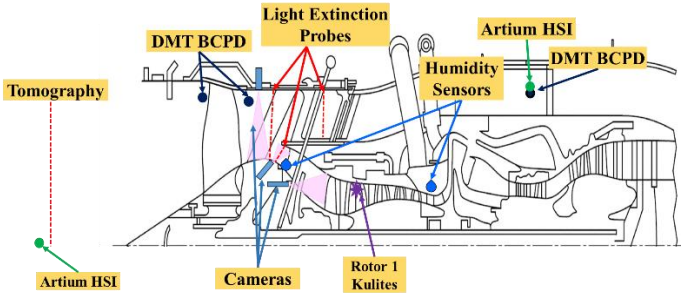

Figure 5. Icing Instrumentation Schematic.

Table 3. Nominal Engine and Flight Test Conditions.

Sweep Series	Reading #	Altitude	Mach, flight	Fan Speed, N1	Temp., ambient, T_{amb}
-	-	kft	-	%	°F
I	188	30	0.6	94	-29
	189	30	0.6	94	-29
	191	30	0.6	94	-29
II	196	30	0.8	70	-32
	197	30	0.8	70	-32
	198	30	0.8	70	-32
III	208	40	0.8	92	-31
	209	40	0.8	92	-31

Table 4. Cloud Conditions

Sweep Series	Reading #	Notional MVD¥	TWC, inlet	Twb* splitter	Twb* IGV
-	-	μm	g/m^3	°F	°F
I	188	small	2.9	31.8	33.2
	189	medium	2.9	-	-
	191	large	2.9	30.5	32.1
II	196	small	1.6	31.6	32.8
	197	medium	1.6	-	-
	198	large	1.6	-	-
III	208	small	1.0	34.0	34.9
	209	large	0.8	34.3	35.1

*** Calculated using COMDES-MELT, empty cells are conditions not calculated in [25]**

¥ MVD size dependent on the tunnel conditions

EXPERIMENTAL RESULTS

Several ice crystal icing investigations were conducted over the course of the Honeywell Uncertified Research Engine test including: the effects of particle size, altitude, inlet cloud uniformity, and inlet relative humidity. Additionally, for each altitude, sensitivity studies were conducted over a range of total water content, ambient temperature, and fan speed. The results discussed below are limited to the effects of particle size.

Particle Size Distributions

Particle size distribution sweeps were obtained for three engine and flight conditions. The percentile cumulative volume diameter (dv) results from the HSI measurements at the engine inlet and in the engine bypass are shown in Table 5. Because of the HSI's limitation on the lower end of the particle spectrum, only $d_{v,0.50}$ and $d_{v,0.99}$ of the particle size distributions are shown. Sample particle size distribution for Sweep I is shown in Figure 6a-c. This sweep had the largest engine inlet $d_{v,0.50}$ range, from 15 to 114 μm.

It can be seen from Table 5 that for each case, particles in the bypass are smaller than the incoming particles at the inlet due to break-up from the fan. For the smaller inlet particle distributions for Readings 188 and 196, there is minimal change in the bypass. Smaller particles may exist but as noted in [33] this is likely attributed to instrumentation limitations. It can be seen that the bypass distributions are very similar for each sweep with the largest inlet distribution of each sweep resulting in only slightly larger distributions in the bypass.

In Sweep I, where the distributions had the largest inlet particle size range from 15 to 114 μm, the bypass distributions were very similar. This may be the effect of the fan speed, which was at 94%, causing increased particle break-up. Another look at fan speed, Sweep II and Sweep III have similar Mach and inlet temperature conditions but the fan speed varied from 70% in Sweep II compared to 92% in Sweep III. For the higher fan speed case in Sweep III, the particle distribution for $d_{v,0.99}$ were very similar whereas for Sweep II at the slower fan speed saw a larger $d_{v,0.99}$ range.

It is recognized that these bypass measurements do not capture what is actually entering the core flowpath and it is speculated that the particle sizes entering the core would be much smaller as the larger particles would be centrifuged into the bypass. Rigby et. al [34] performed LEWICE3D particle trajectory, impact and breakup predictions for several of these test points. The prediction results were compared to the experimental results in the bypass and showed the core ingested significantly smaller particles on the order of 7 μm.

Table 5. Particle Distribution Measurements for MVD Sweeps

Sweep	Reading	Engine Inlet		Engine Bypass	
		$d_{v,0.50}$	$d_{v,0.99}$	$d_{v,0.50}$	$d_{v,0.99}$
I	188	15	31	17	33
	189	45	104	18	34
	191	114	314	28	45
II	196	27	46	20	35
	197	40	92	28	47
	198	51	134	32	58
III	208	31	59	15	25
	209	64	182	17	31

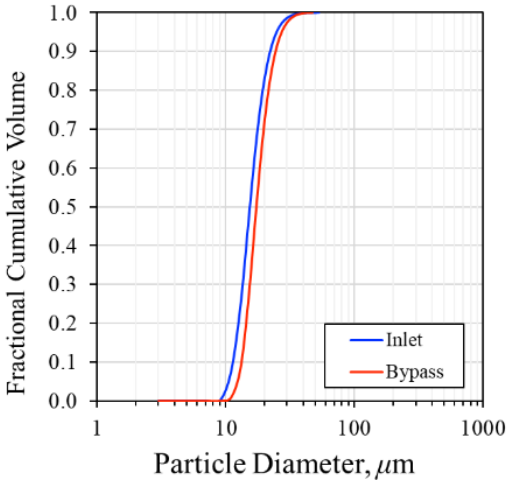

a.) Reading 188, "small" inlet particle distribution.

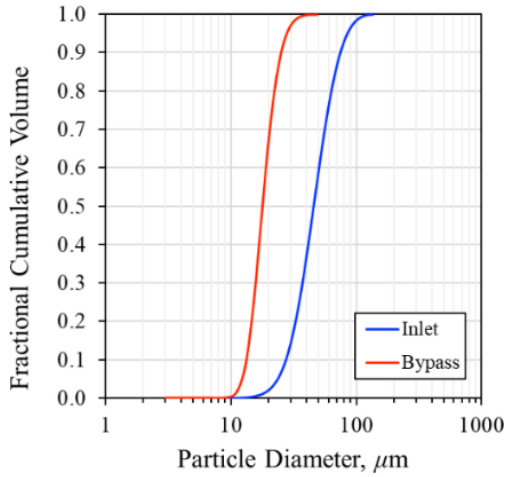

b.) Reading 189, "medium" inlet particle distribution.

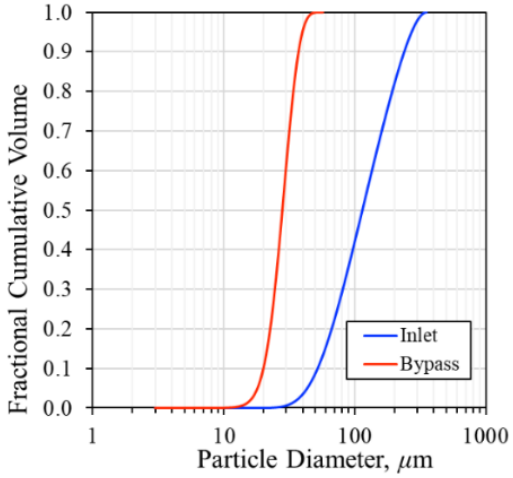

c.) Reading 191, "large" inlet particle distribution.

Figure 6. Sweep I Particle Distribution.

Accretion Characteristics

Cameras focused on the fan exit stator, splitter lip, and inlet guide vanes and were used to capture the ice accretion for the particle size sweeps. Nominal camera placements and views are shown in Figure 7.

Sweep I, with conditions described in Tables 3-5, had inlet $d_{v0.50}$ values ranging from 15μm to 114μm. These conditions showed accretion (Fig. 8) on the pressure side of the exit stator vanes, as indicated by the red circles. Qualitatively, the accretions look very similar across the three particle distributions. The smallest initial distribution shows a slightly larger surface area of accretion.

Downstream of the exit stators at the splitter lip, the accretion (Fig. 9) show similar behavior for all three test points in Sweep I. There are traces of runback water going into the core with three small areas of accretion on the leading edge of the splitter lip and on the total pressure probe for all three particle distributions (Fig. 9a-9c). It should be noted, one of the accretion areas in Fig. 9 is washed out from the lighting but can be observed in the video. For Reading 188 ($d_{v,0.50}$ = 15 μm), as soon as the cloud is initiated, there is immediate water runback and a high frequency build and shed. As the engine metal temperatures stabilize, the shed frequency begins to slow down but still maintains a steady build and shed. Fig 9a is a snapshot that shows the buildup on the splitter lip and total pressure probe. A similar phenomenon is observed for Readings 189 and 191, the initial build up and shedding is very quick and slows over time. However, all three distributions do not produce a firm ice that remains attached during the run.

Moving downstream through the "gooseneck" and to the inlet guide vane (IGV), the accretion begins to look different across the three distributions of Sweep I, as shown in Figure 10. At this area of the engine the environment becomes warmer, promoting more evaporation and melt. For Reading 188 ($d_{v,0.50}$ = 15 μm), six seconds after the ice cloud is activated, accretion near the leading edge on the pressure side of the IGV begins to form. Ice accretion across the three IGV views can be seen in the video. Similarly, for Reading 189 ($d_{v,0.50}$ = 45 µm) IGV accretion can be seen (Fig 10b). However, accretion initiated 16 seconds after the cloud was turned on and does not cover as much of the span as the previous test point. For both cases, the accretion is biased towards the tip region, or outer casing region. As the inlet particle size increases, Reading 191 ($d_{v,0.50}$ = 114 µm), no accretion is observed on the IGV (Figure 10c). It is suggested that as particle sizes increase, there is less melt water. This could be due to fewer smaller particles entering the core. This leads to less evaporative cooling and contact with cold water which increases the metal temperatures. The temperature characteristics will be discussed in more detail in the next section.

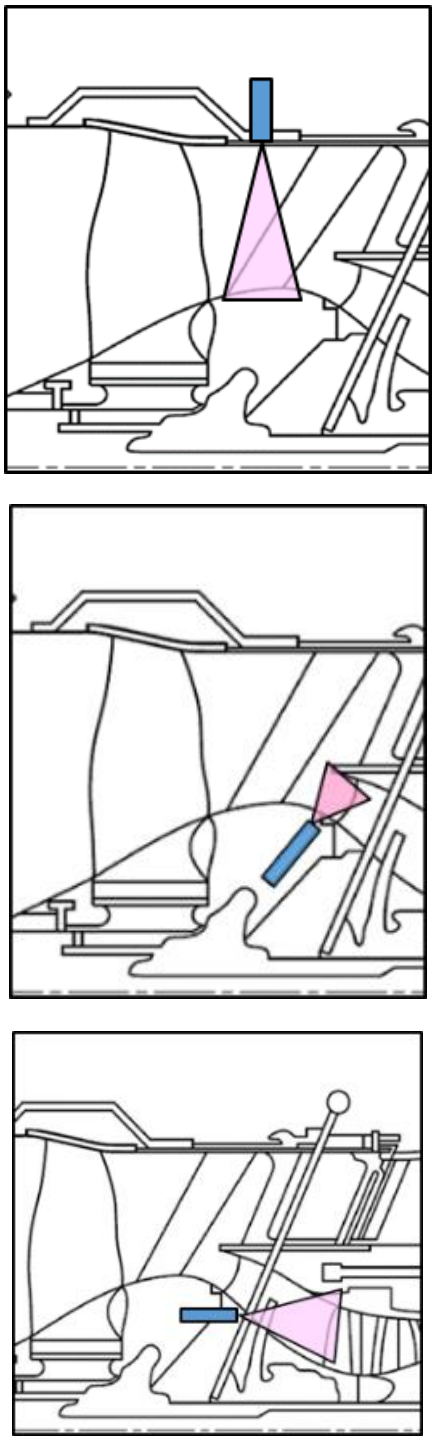

Figure 7. Camera placement to view the Fan Exit Stator Vane (Top), Splitter Lip (Middle), and Inlet Guide Vane (Bottom) views.

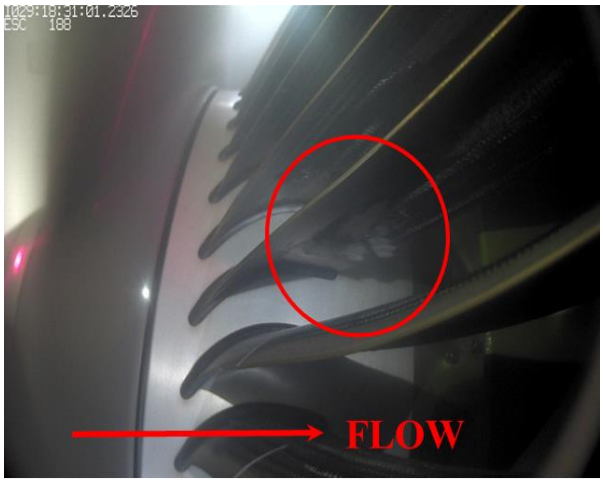

a.) Reading 188, MVD = $d_{v,0.50}$ = 15 μm

b.) Reading 189, MVD = $d_{v,0.50}$ = 45 μm

c.) Reading 191, MVD = $d_{v,0.50}$ = 114 µm

Figure 8. Ice Accretion on the Fan Exit Stator for Sweep I.

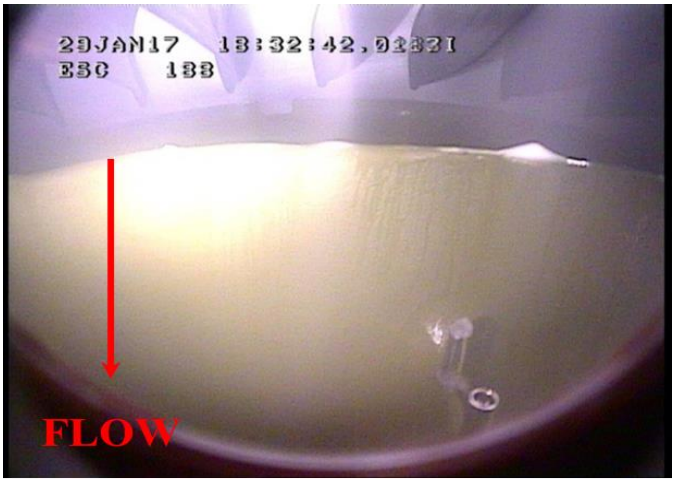

a.) Reading 188, MVD = $d_{v,0.50}$ = 15 μm

b.) Reading 189, MVD = $d_{v,0.50}$ = 45 μm

c.) Reading 191, MVD = $d_{v,0.50}$ = 114 µm

Figure 9. Ice Accretion on the Splitter Lip for Sweep I.

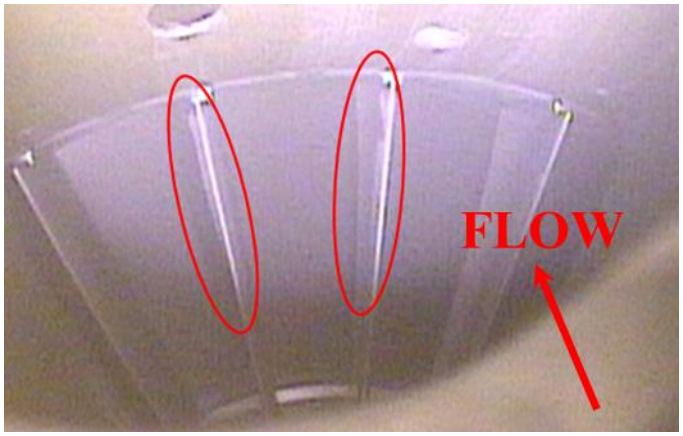

a.) Reading 188, MVD = $d_{v,0.50}$ = 15 μm

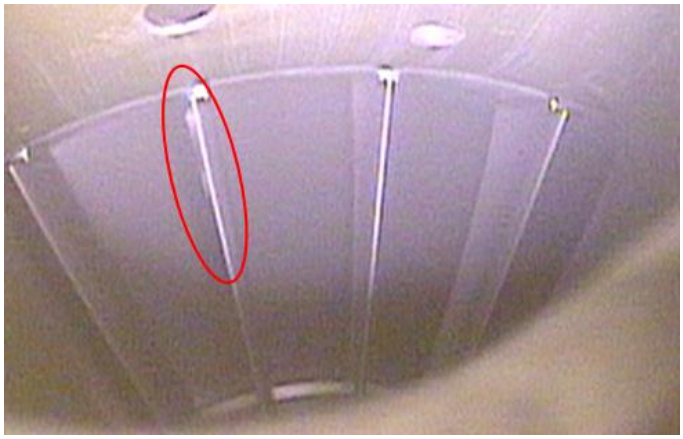

b.) Reading 189, MVD = $d_{v,0.50}$ = 45 μm

c.) Reading 191, MVD = $d_{v,0.50}$ = 114 µm

Figure 10. Ice Accretion on the Inlet Guide Vane for Sweep I.

Temperature Trends

To understand the mechanisms of ice accretion and how it is affected by the incoming cloud, metal temperatures were obtained on the IGV, Vane 1, and Vane 2. Additionally, total temperatures were acquired just aft of the fan and at the compressor discharge. The temperature data for Sweep I is shown in Figures. 11-16. These represent the temperature differences relative to the smallest MVD temperature (i.e. $T_{MVD,I} - T_{MVD,smallest}$).

Metal Temperatures—To ensure the engine wall temperatures reached a new steady state, the temperatures described are the average temperature over the last 10 seconds before the ice cloud was turned off. It can be seen that the IGV (Fig. 11), Vane 1 (Fig. 12), and Vane 2 (Fig. 13) temperature differences increase with increasing MVD (i.e. the metal temperatures are warmer with increasing particle size). Note, these temperatures are shown at the four circumferential locations. The influence of particle size is more pronounced as the metal temperatures go from the IGV towards Vane 2. The temperature trends for Sweeps II and III can be found in the tables in the appendix which show similar trends.

To verify the initial conditions were constant for each MVD, the initial dry condition temperatures prior to the cloud initiating are examined. Figure 14 shows the temperatures for Sweep I which were nearly constant. This is to ensure the initial temperatures are near identical for the sweeps as this could affect the accretion and temperature behavior when the cloud is on. The temperature differences ranged from 0.7°-2.8°F for Sweep I, 0.5°-2.2°F for Sweep II, and 0.06°-1.0°F for Sweep III.

The metal temperatures were compared to the initial dry condition temperatures and found that the temperature drop was larger at the smaller MVD, indicating that the engine surfaces are seeing more liquid water. Suggesting that a larger concentration of smaller particles are making its way into the hidden core and melting.

Total Temperatures—Figure 15 and 16 show the total temperature at the fan exit and compressor discharge exit. It can be seen that the total temperatures remain constant at the fan exit and there is a more notable increase in the compressor exit due to the particle size. Not shown in this paper, comparing the "Cloud On" total temperatures to the initial dry conditions, the aft of fan temperatures only decrease by 4-5°F. This difference decreases with increasing MVD. Likewise, the compressor discharge temperature decreases when the engine ingests the ice particles however the temperature drop minimized with increasing MVD. This suggests that there is a decrease in particles entering the core. This suggest that there is a decrease in the amount of particles entering the core for the larger MVD cases, which decreases the evaporative potential and results in warmer total air temperatures compared to the smaller MVD cases.

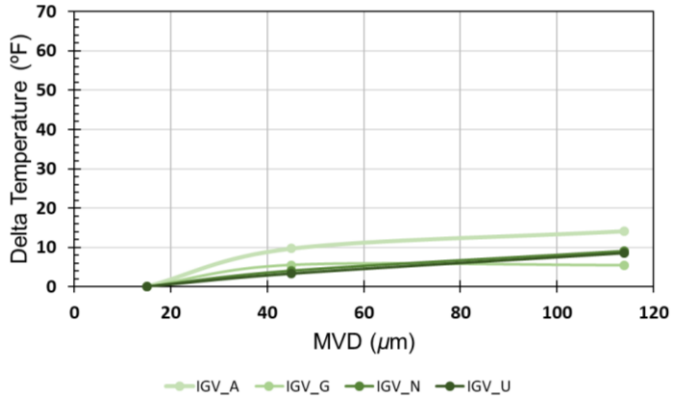

Figure 11. IGV Delta Metal Temperature vs. MVD for Sweep I.

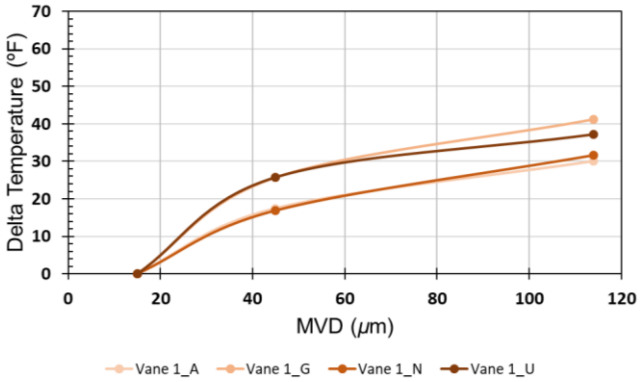

Figure 12. Vane 1 Delta Metal Temperature vs. MVD for Sweep I.

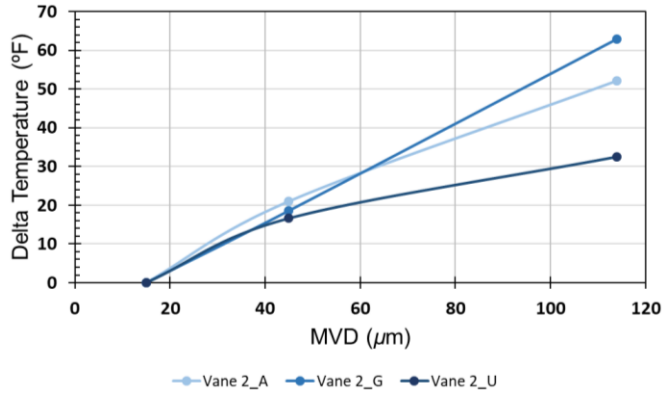

Figure 13. Vane 2 Delta Metal Temperature vs. MVD for Sweep I. (Note: Vane 2_N not available)

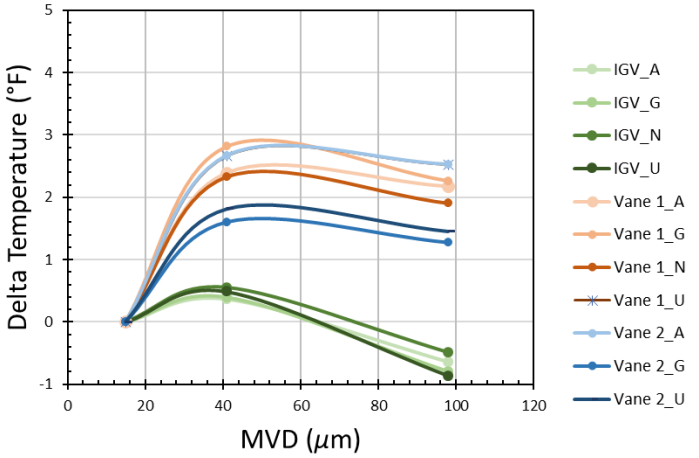

Figure 14. Sweep I Dry Condition Core Delta Temperatures.

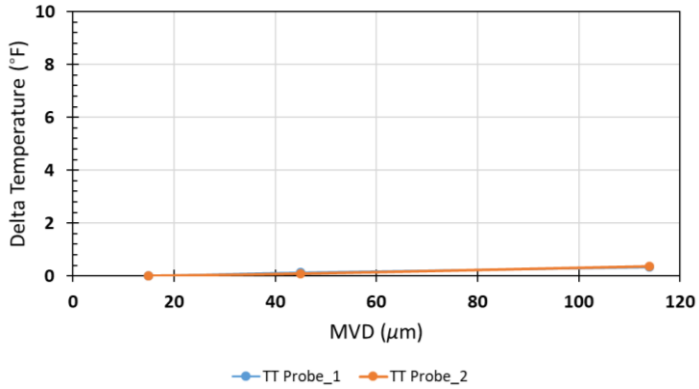

Figure 15. Aft Fan Delta Total Temperature vs. MVD for Sweep I.

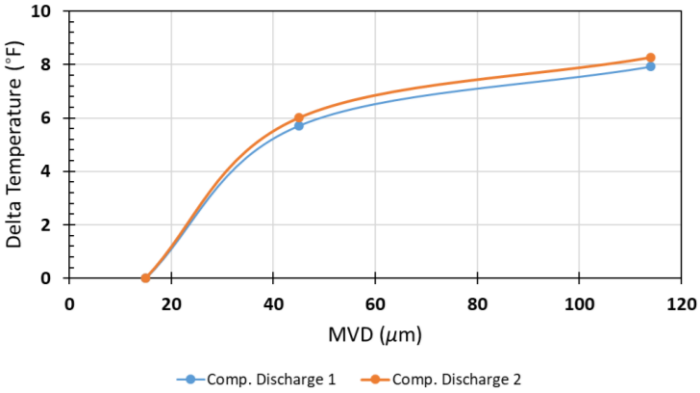

Figure 16. Compressor Discharge Delta Total Temperature vs. MVD for Sweep I.

DISCUSSION

The accretion videos and temperature trend show that particle size presented at the fan inlet will result in different break-up characteristics that will affect the accretion behavior. The video data shows that at the largest MVD for Sweep I, the conditions did not result in accretion. Coupling that with the metal temperatures, the metal temperatures do not decrease as much as the smaller MVD cases. This could be due to less smaller particles entering the core and melting providing either the liquid or evaporative cooling needed to begin the accretion process. It is still not conclusive if the temperature rise is due to less overall particle concentration getting into the core, more larger particles, etc. Not described in this paper, it was found that the mass mixing ratio (MMR) data from the humidity sensor located on the engine front frame, the MMR had a slight increase with increasing MVD. More information coupled with the humidity is still needed to make a stronger conclusion.

Follow-on work should look at obtaining total water content measurements from the Light Extinction Probes to understand how much water and ice is entering the core and bypass. A preliminary look of the raw light extinction probe signals show the extinction at the bypass entrance decreases with increasing MVD. It is not well understood how the extinction would change due to larger particle size versus less concentration of smaller particles. It is thought that the smaller particles will follow the flow stream, having more ability to make it into the hidden core compared to the larger particles. Improvements in particle sizing technology to capture particles smaller than 15μm would also help shed light on the full distribution of particles entering the core and bypass.

Additionally, the results from this test show that particle size should be considered when setting up for an engine test in an icing facility. The icing risk criteria used for the 1D Icing Risk Analysis tool [10] shows a very narrow band of wet bulb temperatures can lead to ice accretion. This study indicated that just by changing the inlet particle size can impact that temperature band. Additionally, the hidden core configuration could exacerbate the particle size effects due to the likelihood of more particles entering the bypass. For an example [20] a previous engine test shows little particle size effect until there was a threshold region of accretion.

CONCLUSIONS

A Honeywell Uncertified Research Engine was tested under ice crystal icing conditions in the Propulsion Systems Laboratory. The data was used to develop NASA's 1D Icing Risk Analysis tool and 3D icing simulation tools. Data was acquired over a wide range of conditions to understand the primary drivers effecting accretion in turbofan engines. This study also looked at improving measurement techniques to enable quantitative icing measurements in an engine environment.

An interest in the icing community is to understand particle break-up in an engine and from a facility operation perspective, there is an interest to understand how particle size variations at

the engine inlet will change the engine characteristics. Three particle size sweeps were conducted for three different engine and flight conditions. Due to the freeze out method the facility uses to fully glaciate the ice particles, spherical particles are produced.

Particle sizing data, images of the areas of interest (for ice accretion), and temperature trends in the engine were observed. This was the first time during an engine test that particle sizing data was acquired due to the complexity of both the typical instruments used and the engine environment being sampled. It was found that the initial particle size does effect the accretion behavior in this hidden core geometry.

The data from the particle size imaging instruments (Artium HSI) installed upstream of the engine and in the bypass show that the particles do break-up into smaller distributions in the bypass. For Sweep I, which had the largest inlet particle size range from 15 to 114 μm, the bypass distributions were very similar. This could be attributed to the high fan speed compared to the other particle size sweeps.

The accretion behavior observed in the videos looking at the fan exit stator, splitter lip, and IGV showed that the accretion behavior was very similar in the front of the engine at the fan stator and splitter lip. However, at the IGVs, the accretion decreased with increasing particle size where the largest MVD resulted in no accretion.

The metal temperatures at the IGV, Vane 1, and Vane 2 show that the particle size effects were more prominent further down the engine at Vane 2. The metal temperatures increased with increasing MVD.

The data from the video and thermocouples indicates that the break-up from the fan and the hidden core geometry result in less particle melt which is needed for heavy accretion to occur. This could be due to the larger particles being more ballistic and are more likely to centrifuge into the bypass even after particle break-up. This was the first time particle size measurements were made inside an engine flow path and it provided insight on the particle break-up phenomenon in a realistic engine environment. More work is still needed to understand the primary contributors affecting the accretion characteristics.

ACKNOWLEDGEMENTS

This work was supported under the NASA Advanced Air Vehicles Program, Advanced Air Transport Technology Project and the Aeronautics and Evaluation Test Capability Project. The author would like to thank Michael King for developing a method to acquire and process the HSI particle size data in an engine environment. Thank you to Peter Struk, Tadas Bartkus, Juan Agui, and Paul Tsao for technical guidance and test support, and the rest of the Engine icing team for their expertise. The author would also like to acknowledge Dr. Judith Van Zante for providing icing cloud expertise, Tim Bencic for developing and acquiring the advanced instrumentation measurements, and Joe Veres and Phil Jorgenson for providing COMDES-MELT results, and to the entire PSL staff for their dedication and support of this test. The author also wishes to thank Nicci Reising, Dave Dischinger, Bob Ciero, Steven Craver, Paul Gustafson, Terry Neal, Dan Walker, Wolfgang Sandel, and the rest of the Honeywell team for their contributions during the engine test.

REFERENCES

[1] Struk, P., Currie, T., Wright, W. B., Knezevici, D. C., Fuleki, D., Broeren, A., Vargas, M., and Tsao, J. "Fundamental Ice Crystal Accretion Physics Studies," SAE 2011 International Conference on Aircraft and Engine Icing and Ground Deicing, SAE Technical Paper 2011-38-0018 or NASA/TM-2012-217429, 2011.

[2] Currie, T. C., Struk, P. M., Tsao, J., Fuleki, D., and Knezevici, D. C. "Fundamental Study of Mixed-Phase Icing with Application to Ice Crystal Accretion in Aircraft Jet Engines," 4th Atmospheric and Space Environments Conference, AIAA 2012-3035, 2012.

[3] Struk, P. M., Bencic, T., Tsao, J., Fuleki, D., and Knezevici, D. C. "Preparation for Scaling Studies of Ice-Crystal Icing at the NRC Research Altitude Test Facility," 5th AIAA Atmospheric and Space Environments Conference, AIAA-2013-2675 and NASA/TM-2013-216571, 2013.

[4] Struk, P. M., Bartkus, T. P., Tsao, J. C., Currie, T., and Fuleki, D. "Ice Accretion Measurements on an Airfoil and Wedge in Mixed-Phase Conditions," SAE 2015 International Conference on Icing of Aircraft, Engines, and Structures, SAE Technical Paper 2015-01-2116, 2015.

[5] Struk, P. M., Tsao, J. C., and Bartkus, T. P., "Plans and Preliminary Results of Fundamental Studies of Ice Crystal Icing Physics in the NASA Propulsion Systems Laboratory," 8th AIAA Atmospheric and Space Environments Conference, AIAA-2016-3738, 2016.

[6] Struk, P. M., Ratvasky, T. P., Bencic, T. J., Van Zante, J. F., King, M. C., Tsao, J. C., and Bartkus, T. P., "An Initial Study of the Fundamentals of Ice Crystal Icing Physics in the NASA Propulsion Systems Laboratory," 9th AIAA Atmospheric and Space Environments Conference, American Institute of Aeronautics and Astronautics, AIAA 2017-4242, 2017.

[7] Veres, J. P., Jorgenson, P. C. E., "Modeling Commercial Turbofan Engine Icing Risk with Ice Crystal Ingestion," 5th AIAA Atmospheric and Space Environments Conference, San Diego, CA, June 24-27, 2013, AIAA 2013-2679 and NASA/TM-2013-218097.

[8] Jorgenson, P. C. E., Veres, J. P., Coennen, R., "Modeling of Commercial Turbofan Engine with Ice Crystal Ingestion; Follow-On," 6th AIAA Atmospheric and Space Environments Conference, Atlanta, GA, June 16-20, 2014, AIAA-2014-2899 and NASA/TM-2014-218496.

[9] Veres, J.P., Jones, S.M., Jorgenson, P.C.E., "Performance Modeling of Honeywell Turbofan Engine Tested with Ice Crystal Ingestion in the NASA Propulsion System Laboratory," SAE 2015 International Conference on Aircraft and Engine Icing and Ground Deicing, 2015-01-2133.

[10] Veres, J.P., Jorgenson P. C. E., Jones, S. M., "Modeling of Highly Instrumented Honeywell Turbofan Engine Tested with Ice Crystal Ingestion in the NASA Propulsion System Laboratory," *8th AIAA Atmospheric and Space Environments Conference*, Washington, D.C, June 13-17, 2016.

[11] Veres, J.P., Jorgenson, P.C.E., Jones, S.M., Nili, S., "Modeling of a Turbofan Engine with Ice Crystal Ingestion in the NASA

Propulsion Systems Laboratory," *ASME IGTI 2017 Turbo Expo*, Charlotte, NC, June 26-30,2017, GT2017-63202.
[12] Knezevici, D. C., Fuleki, D., Currie, T. C., Galeote, B., Chalmers, J., and MacLeod, J. D. "Particle Size Effects on Ice Crystal Accretion - Part II," *5th AIAA Atmospheric and Space Environments Conference*, AIAA-2013-2676, 2013.
[13] Hauk, T., Roisman, I. V., and Tropea, C. D. "Investigation of the Impact Behaviour of Ice Particles," *6th AIAA Atmospheric and Space Environments Conference*, AIAA-2014-3046, 2014.
[14] Hauk, T., Bonaccurso, E., Roisman, I. V., and Tropea, C. "Ice crystal impact onto a dry solid wall. Particle fragmentation," *Proceedings of the Royal Society of London A: Mathematical, Physical and Engineering Sciences* Vol. 471, No. 2181, 2015.
[15] Vargas, M., Ruggeri, C., Pereira, M., Revilock, D., "Ice Particles Impacting on a Flat Plate: Temperature and Velocity effect," *12th AIAA Atmospheric and Space Environments Conference*, Reno, NV, June 15-19, 2020, submitted abstract.
[16] Hauk, T. "Investigation of the Impact and Melting Process of Ice Particles." Technischen Universität Darmstadt, 2016.
[17] Vargas, M., Struk, P. M., Kreeger, R. E., Palacios, J., Iyer, K., and Gold, R. E. "Ice Particle Impacts on a Moving Wedge," *6th AIAA Atmospheric and Space Environments Conference*, AIAA-2014-3045, 2014.
[18] Oliver, M. J. "Validation Ice Crystal Icing Engine Test in the Propulsion Systems Laboratory at NASA Glenn Research Center," *6th AIAA Atmospheric and Space Environments Conference*, AIAA-2014-2898, June 2014.
[19] Goodwin, R.V., Dischinger, D.G., "Turbofan Ice Crystal Rollback Investigation and Preparations Leading to Inaugural Ice Crystal Engine Test at NASA PSL-3 Facility," *6th AIAA Atmospheric and Space Environments Conference*, AIAA-2014-2895, 2014.
[20] Flegel, A.B., Oliver, M.J., "Preliminary Results from a Heavily Instrumented Engine Ice Crystal Icing Test in a Ground Based Altitude Test Facility," *8th AIAA Atmospheric and Space Environments Conference*, Washington, D.C, June 13-17, 2016, AIAA 2016-3894. NASA/TM-2016-29132.
[21] Goodwin, R.V., Fuleki, D., "Turbofan Ice Crystal Rollback Investigation and Preparations Leading to the Second, Heavily Instrumented, Ice Crystal Engine Test at NASA PSL-3 test Facility," *8th AIAA Atmospheric and Space Environments Conference*, Washington, D.C, June 13-17, 2016, AIAA-2016-3892.
[22] Bidwell, C., and Rigby, D. L. "Ice Particle Analysis of the Honeywell ALF502 Engine Booster," *SAE 2015 International Conference on Icing of Aircraft, Engines, and Structures* 2015-01-2131, 2015.
[23] Rigby, D. L., Ameri, A. A., Veres, J., Jorgenson, P. C. E., "Viscous Three-Dimensional Simulation of Flow in an Axial Low Pressure Compressor at Engine Icing Operating Points," *9th AIAA Atmospheric and Space Environments Conference*, Denver, CO, June 5-9, 2017, AIAA-2017-4087.
[24] Rigby, D. L., Wright, W.B., "Numerical Investigation of Particle Breakup and Ingestion into an Axial Low Pressure Compressor at Engine Icing Operating Points," *10th AIAA Atmospheric and Space Environments Conference*, Atlanta, GA, June 25-29, 2018, AIAA-2018-4131.
[25] Jorgenson, P.C.E., Veres, J.P., Bommireddy, S.R., Nili, S., "Analysis of the Honeywell Uncertified Research Engine (HURE) With Ice Crystal Cloud Ingestion at Simulated Altitudes: Public Version," NASA/TM—2018-220023.
[26] Leroy, D., E. Fontaine, A. Schwarzenboeck, J. W. Strapp, A. Korolev, G. McFarquhar, R. Dupuy, C. Gourbeyre, L. Lilie, A. Protat, J. Delanoe, F. Dezitter and A. Grandin, "Ice crystal sizes in High Ice Water Content clouds. Part 2 : Statistics of Median Mass Percentiles in Tropical Convection Observed during the HAIC/HIWC project. J.Atmospheric Ocean. Technol. https://doi.org/10.1175/JTECH-D-15-0246.1
[27] Griffin, T. A., Lizanich, P., and Dicki, D. J. "PSL Icing Facility Upgrade Overview," 6th AIAA Atmospheric and Space Environments Conference, AIAA-2014-2896, 2014.
[28] PSL Customer Guide to be submitted as NASA TM
[29] 14 CFR Parts 25 and 33: Airplane and Engine Certification Requirements in Supercooled Large Drop, Mixed Phase, and Ice Crystal Icing Conditions, Final Rule, Federal Register, Vol. 79, No. 213, November 4, 2014, 2014-25789.
[30] Van Zante, J. F., Ratvasky, T. P., Bencic, T. J., Challis, C. C., et al., "Update on the NASA Glenn Propulsion Systems Lab Icing and Ice Crystal Cloud Characterization - 2017," *10th Atmospheric and Space Environments Conference*, AIAA 2018-3969, 2018.
[31] PSL Measurement Uncertainty Analysis to be submitted as NASA TM
[32] Bencic, T.J., Fagan, A.F., Van Zante, J.F., Kirkegaard, J.P., Rohler, D.P., Maniyedath, A., Izen, S.H., "Advanced Optical Diagnostics for Ice Crystal Cloud Measurements in the NASA Glenn Propulsion Systems Laboratory," *5th AIAA Atmospheric and Space Environments Conference*, (AIAA 2013-2678)
[33] King, M.C., Flegel, A. B., Manin, J., "Particle Size Measurements from the 2018 Honeywell Uncertified Research Engine Test in the NASA Propulsion System Laboratory," *NASA/TM—2020-XXXXX*.
[34] Rigby, D. L., Wright, W.B., Flegel, A.B., King, M.C., "Simulation of Ice Particle Breakup and Ingestion into the Honeywell Uncertified Research Engine (HURE)," *SAE International Icing Conference*, 2019-01-0159.

T3_2	°F	0.0	5.6	2.2

Appendix –Delta Temperature Trends

Table 6. Sweep I Delta Temperatures.

Sweep I				
MVD, $d_{v0.50}$	µm	15	45	114
RDG	-	188	189	191
Aft Fan 1	°F	0.0	0.1	0.3
Aft Fan 2	°F	0.0	0.1	0.4
IGV_A	°F	0.0	9.7	14.1
IGV_G	°F	0.0	5.5	5.4
IGV_N	°F	0.0	4.1	9.1
IGV_U	°F	0.0	3.3	8.5
Vane 1_A	°F	0.0	17.4	30.0
Vane 1_G	°F	0.0	25.7	41.2
Vane 1_N	°F	0.0	16.9	31.7
Vane 1_U	°F	0.0	25.8	37.2
Vane 2_A	°F	0.0	21.0	52.2
Vane 2_G	°F	0.0	18.6	62.9
Vane 2_U	°F	0.0	16.6	32.5
T3_1	°F	0.0	5.7	7.9
T3_2	°F	0.0	6.0	8.3

Table 7. Sweep II Delta Temperatures.

Sweep II				
MVD, $d_{v0.50}$	µm	27	40	51
RDG	-	196	197	198
Aft Fan 1	°F	0.0	2.7	13.8
Aft Fan 2	°F	0.0	2.7	13.7
IGV_A	°F	0.0	6.1	4.2
IGV_G	°F	0.0	6.4	5.0
IGV_N	°F	0.0	6.5	4.5
IGV_U	°F	0.0	6.3	4.8
Vane 1_A	°F	0.0	30.1	34.1
Vane 1_G	°F	0.0	30.4	29.1
Vane 1_N	°F	0.0	32.5	19.6
Vane 1_U	°F	0.0	27.9	27.9
Vane 2_A	°F	0.0	23.5	46.6
Vane 2_G	°F	0.0	31.6	76.9
Vane 2_U	°F	0.0	44.0	85.8
T3_1	°F	0.0	5.5	2.0

Table 8. Sweep III Delta Temperatures.

Sweep III			
MVD, $d_{v0.50}$	µm	31	64
RDG	-	208	209
Aft Fan 1	°F	3.5	6.2
Aft Fan 2	°F	3.6	6.3
IGV_A	°F	7.5	13.6
IGV_G	°F	6.6	10.6
IGV_N	°F	6.3	12.2
IGV_U	°F	5.4	12.4
Vane 1_A	°F	49.6	66.4
Vane 1_G	°F	52.6	72.1
Vane 1_N	°F	54.6	75.2
Vane 1_U	°F	49.0	64.9
Vane 2_A	°F	83.1	113.0
Vane 2_G	°F	67.5	85.9
Vane 2_U	°F	76.7	97.6
T3_1	°F	25.6	37.3
T3_2	°F	27.4	39.2